applied sciences

MDPI

Article

Pentane Depletion by a Surface DBD and Catalysis Processing

Cecilia Piferi [1], Matteo Daghetta [1], Marco Schiavon [2], Hector Eduardo Roman [1] and Claudia Riccardi [1,*]

[1] Dipartiment of Physics, University of Milano-Bicocca, Piazza della Scienza 3, 20126 Milano, Italy; c.piferi@campus.unimib.it (C.P.); matteo.daghetta@unimib.it (M.D.); hector.roman@unimib.it (H.E.R.)
[2] Department of Civil, Environmental and Mechanical Engineering, University of Trento, via Mesiano 77, 38123 Trento, Italy; marco.schiavon@unitn.it
* Correspondence: claudia.riccardi@unimib.it

Abstract: We study pentane depletion using a hybrid plasma system based on a surface dielectric barrier discharge (SDBD), with and without a catalyst, and as a function of plasma power and alkane concentration. We evaluate pentane decomposition efficiency based on plasma power and quantify the role of the catalyst in the resulting depletion of intermediate products. Analyses of the temporal evolution of pentane and the intermediate decomposition products allow us to estimate the corresponding decomposition rates according to the plasma parameters. We find that depletion efficiency increases as a function of pentane concentration. Furthermore, it is shown that the catalytic processes are responsible for a significant increase in the depletion rates of the intermediate reaction products, thus contributing to the total abatement process of pentane.

Keywords: surface dielectric barrier discharge; atmospheric pressure; Non-Thermal Plasmas; streamer discharge; pentane and VOC abatement

check for updates

Citation: Piferi, C.; Daghetta, M.; Schiavon, M.; Roman, H.E.; Riccardi, C. Pentane Depletion by a Surface DBD and Catalysis Processing. *Appl. Sci.* **2022**, *12*, 4253. https://doi.org/10.3390/app12094253

Academic Editor: Xinpei Lu

Received: 22 March 2022
Accepted: 21 April 2022
Published: 22 April 2022

Publisher's Note: MDPI stays neutral with regard to jurisdictional claims in published maps and institutional affiliations.

1. Introduction

One of the most important environmental issues at present is air pollution, which can be harmful to both the environment and to human health. Thanks to recent strict regulations, emissions of atmospheric pollutants have been reduced significantly during the last decades, especially in heavily industrialized countries. Despite all these efforts, the concentrations of pollutants within large urban zones remain too high, particularly in developing countries, and further improvement in atmospheric air quality is required. This can be accomplished by encouraging more specific studies [1].

A large and important group of pollutants is the volatile organic compounds (VOCs); due to their high volatility, these compounds rapidly evaporate, thus easily leaving the places where they are produced and diffusing into the atmosphere. It is now well-understood that they can cause a variety of deleterious effects to human health and the environment [2]. VOCs are mostly emitted during industrial processing in different types of mixtures with air, where the magnitude of fluxes ranges from 1000 m^3/h to approximately 10,000 m^3/h.

Different methods for VOC depletion are being tested on pilot plants, with some already being employed in industries, including: adsorption [3], absorption [4], thermal decomposition [5], catalytic oxidation [6], bio-filtration [7], and membrane separation [8]. Most of these technologies present several economic and efficiency limitations when treating effluents with low VOC concentrations, high airflow rate, and with compounds that have low solubility in water [9].

Plasma can serve as an alternative in the removal of VOCs from gas streams. Various equilibrium and non-equilibrium plasma reactors are being investigated, and their selective efficiency in VOC abatement has been reported in literature reviews [10,11]. Equilibrium plasmas are also thermal ones, since charges and neutrals are produced at high temperatures of the order of 10^4 K. Thermal plasmas such as torches and arches are employed for different

purposes, including, for instance, in the gasification of coal [12] as well as in the waste gas decomposition of hard-to-convert components such as Perfluorocarbons PFCs [13].

These plasmas have the advantage of high and fast dissociation rates and rather good efficiency, but most of them are characterized by high energetic consumption, which is required to sustain the discharge itself, and high maintenance and equipment costs. They often employ noble gas carriers, liquids, or vapor water [14]. Although they can be used for the abatement of harmful toxic gases, they are economically unsustainable for the abatement of VOCs at low concentrations.

Non-equilibrium plasmas, often called Non-Thermal Plasmas (NTPs), can instead be sustained with lower energy than Thermal Plasmas. NTPs are very weakly ionized and are not in thermodynamic equilibrium because electrons absorb most of the electromagnetic energy, reaching temperatures of several eV, while ionic species and neutral kinetic energies remain at room temperature. For this reason, they are also called cold plasmas. NTPs are generated by using different types of devices such as the dielectric barrier discharge [10], gliding arc discharge [15], microwave plasma [16], and plasma jets [17,18].

Nowadays, they are employed in several environmental applications. For instance, some NTPs such as plasma jets and microwaves are intensively studied for reforming methane and carbon dioxide because of their high efficiency [16], while DBDs are often used for the removal of VOCs at low concentrations, and also for odor abatement in combination with catalysis [19].

Most of the NTP sources working at atmospheric pressure are called Cold Atmospheric Plasmas (CAPs). The abatement phenomena in CAPs are dominated by kinetic effects, where electrons are the primary source of molecular dissociation and radical formation. Then, the resulting chemical reactions between radicals promote their degradation and oxidation in the presence of oxygen species. Compared to the aforementioned thermal plasmas, they are characterized by lower dissociation rates, but not by lower efficiency [9].

As reported in the literature, one of the most employed cold plasma devices is the Dielectric Barrier Discharge, which has the advantage of requiring very low energy. DBDs are also used in combination with catalysis, an example of which is the dielectric packed bed discharge [18]. DBDs, as most of CAPs, have the drawback of processing only small gas volumes. In the DBD configuration, the gas is physically confined to pass between the two electrodes, the plasma state is mostly confined to a volume of a few mL, and gas air flows between a few mL/min and some L/min [9,17]. Only very recently, a system composed of DBDs, a mineral adsorber, and a bio-scrubber [11] has been investigated for gas flows of up to 1000 m^3/min, yielding a good VOC abatement efficiency. The scale-up factors and operating costs need to be investigated in order to evaluate their real economic sustainability in view of the most interesting applications.

A possible way to overcome the difficulty of a redeeming technology on a large scale—that is, treating large gas volumes at low VOC concentrations—could be through the employment of a peculiar CAP: the surface DBD (SDBD) [20]. In SDBDs, the plasma is produced on a surface without being confined between two electrodes. In this new configuration, the gas can move on the surface and rapidly diffuse into larger volumes. Moreover, these devices have not been investigated in such a detail as the DBD and the packed DBD for their waste air remediation applications. Only recently have a few research papers been devoted to the application of SDBDs in VOC abatement [21,22].

Starting from our previous knowledge on DBD [18,23] and SDBD plasmas, this paper presents a study on the performance of a single SDBD module working at static conditions, aimed at evaluating the VOC abatement rates based on the relevant parameters, particularly including possible synergies with post-catalysis processing. More specifically, we employ an asymmetrical SDBD configuration [20] and investigate the chemical kinetics dissociation of a specific VOC in an air mixture while varying its concentrations and plasma energy. We choose pentane as a VOC and whose decomposition by-products are mainly acetylene and propane. The concentration of pentane and its by-products are measured according to time in order to analyze their decay law measured during the experiments. From these results,

we can draw some conclusions about performance efficiencies for different parameters as well as estimate the best possible operating conditions, such as by evaluating the opportunity of using a number of SDBD modules fed in an asymmetrical configuration for specific real applications.

Although NTPs have been largely studied in the last decades for their role in the depletion of VOCs in air, the literature on pentane abatement/conversion is still scarce. To the authors' knowledge, no experiments on the oxidation of pentane in air in low temperature atmospheric pressure plasmas have been reported in the literature. Thus, the present paper describes a novel application of NTP-catalysis and contributes to the enrichment of the available literature.

The paper is organized as follows. In Section 2, we present the experimental setup and briefly discuss the calibration of the gas chromatograph. Section 3 is devoted to the experimental results, and Section 4 presents a discussion of our results as compared to others from the literature. Finally, in Section 5, we conclude with our final remarks.

2. Experimental Setup

The configuration adopted in our experiments, the simplest version of the SDBD used in plasma aerodynamics applications, is called a plasma actuator. It consists of two conducting electrodes attached to the opposite sides of a flat dielectric panel, as seen in the asymmetrical arrangement sketched in Figure 1.

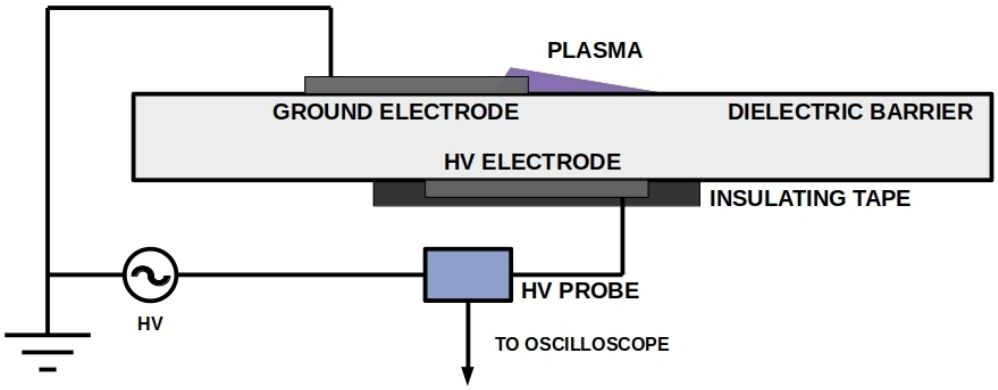

Figure 1. Plasma device scheme: The two electrodes, consisting of deposed copper (35 µm thick, 4 cm wide, and 12 cm long), are attached to a dielectric material and are laterally shifted from each other by about 0.5 cm (typical asymmetry in SDBD). The lower electrode, fed at a high voltage (HV), is covered with an insulating material, whereas the upper one, fed to the ground, is exposed to air. The HV probe measures the applied potential.

The lower electrode is covered with an insulating material, whereas the upper one remains fully exposed to the air. In this way, the plasma generation region is confined above the dielectric plate. For the dielectric barrier, we used a vetronite sheet, with the possibility to change its thickness (1.5–3.0 mm). More specifically, we used a 1.5 mm thick dielectric barrier in vetronite and a pair of 12 cm long conductive electrodes leaning on the two faces of the barrier.

Upon the application of a sufficiently high voltage (HV), the air portion in proximity to the device gets weakly ionized, thus creating a thin plasma layer above the insulating plate, as illustrated in Figure 1. The SDBD plasma actuator generates a non-thermal self-limiting plasma, in which the accumulation of charged particles on the dielectric surface opposes the applied electric field. Consequently, AC or pulsed high voltages are required to have a temporally prolonged discharge operation; otherwise, only a transient air ionization occurs at the voltage ignition.

In the present configuration, the exposed electrode is grounded, whereas the covered one is fed by a high-voltage power supply line. This consists of a DC-voltage supplier and

a signal generator feeding the primary windings of an HV transformer, whose secondary windings are connected to the electrode. We set the reference DC supply voltage (VDC) within the range of 7–14 V. The whole system behaves similarly to a resonant circuit, so the sinusoidal voltage frequency slightly depends on the DC-supply voltage. In this asymmetric configuration, due to the partial overlapping of the electrodes by about a centimeter, a so-called ionic wind is generated, which is a directional flow from the exposed electrode to the buried one.

The SDBD is located in the reactor, a parallelepiped with the size of $1.8 \times 20 \times 18\,cm^3$ made by Delrin and with a cover in Plexiglas (box used for the experiments that has not been attacked by the used VOC or its decomposition products), inside which VOC depletion takes place. The volume of the free space used for the air treatment is about 0.5 L. The experiments were performed in static conditions, as described below. The VOC used in this experiment is pentane (C_5H_{12}), employed at variable concentrations between 300 ppm and 1200 ppm.

The VOC contamination setup is shown in Figure 2. The black bold lines represent the tube connections through the whole system. In the diagram, "Pure air" represents a gas cylinder from Sapio S.R.L. containing 79% N_2 and 21% O_2, which means that the concentration of CO_2 (0.5 ppm), CO (0.5 ppm), hydrocarbons (0.1 ppm), water (3 ppm), and other pollutants is negligible. The red crosses represent ball valves. The liquid pentane is placed in a bubbler bottle (denoted as Liquid VOC in Figure 2) and is allowed to circulate through the flow meter by the action of the air pressure. We used two gas flow meters and one liquid flow meter, all produced by the Bronkhorst factory. The controlled evaporator and mixer (CEM) allow the liquid coming from the liquid flow meter to evaporate and mix with a line of pure air that comes from gas flow meter 1, thus producing the first dilution of pentane. A second dilution is performed after the CEM through the addition of pure air coming from gas flow meter 2. This whole system allows for the control of the chamber pentane concentration before the experiments. Finally, for the gas chromatographic analysis, we used a Micro GC Agilent 3000 instrument with the column PoraPLOT U, which is a column specific for VOCs, and with a Thermal Conductivity Detector (TCD). The program used is as follows: inlet temperature at 70°, inject temperature at 100°, column temperature at 110°, inject time 50 ms, and run time 300 s. The gas chromatograph (GC) samples are of the order of 10^{-3} mL for each time. The GC inlet pipe is placed at about 5 cm after the plasma region.

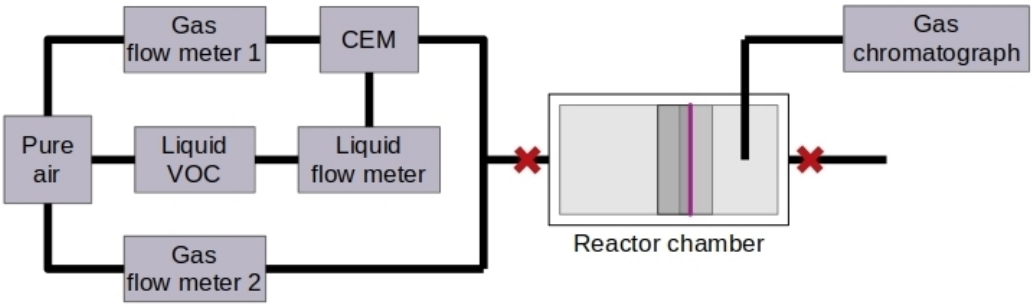

Figure 2. Liquid VOC contamination setup: The pure air cylinder supply for both the gas carriers and the bubbler device containing the VOC. A controlled evaporator and mixer (CEM) allow the liquid to evaporate and then mix with a line of pure air flow. The SDBD is located in the reactor, a parallelepiped with the size of $1.8 \times 20 \times 18\,cm^3$ made by Delrin and with a cover in Plexiglas, inside which VOC depletion takes place. The volume of the free space used for the air treatment is about 0.5 L. The gas chromatographic analysis was performed with a Micro GC Agilent 3000 instrument.

The experiments were performed with and without a catalyst. The catalyst consisted of a dispersion of TiO_2 in an aqueous solution of polyvinyl alcohol (PVA). It was deposited by means of a fine brush, as a strip of 4 cm in width and 12 cm in length, at a distance of 0.3 cm from the exposed copper electrode. After the evaporation of water at room

temperature, the deposition was repeated until a uniform distribution of the product was obtained. A total of 0.2 g of dried catalyst TiO_2 was deposited. In order to prepare the catalyst, 6 g of Ti(IV) oxide anatase 325 mesh (Sigma Aldrich) was carefully added to a solution, initially prepared with the use of 1 g of PVA (Kuraray Poval 10-98) and 100 mL of deionized water. After vigorous stirring, a fluid suspension was obtained, which was stored at room temperature until the deposition. In Figure 3, we show an SEM image of the catalyst where we can clearly identify sub-micrometre TiO_2 particles on the PVA matrix.

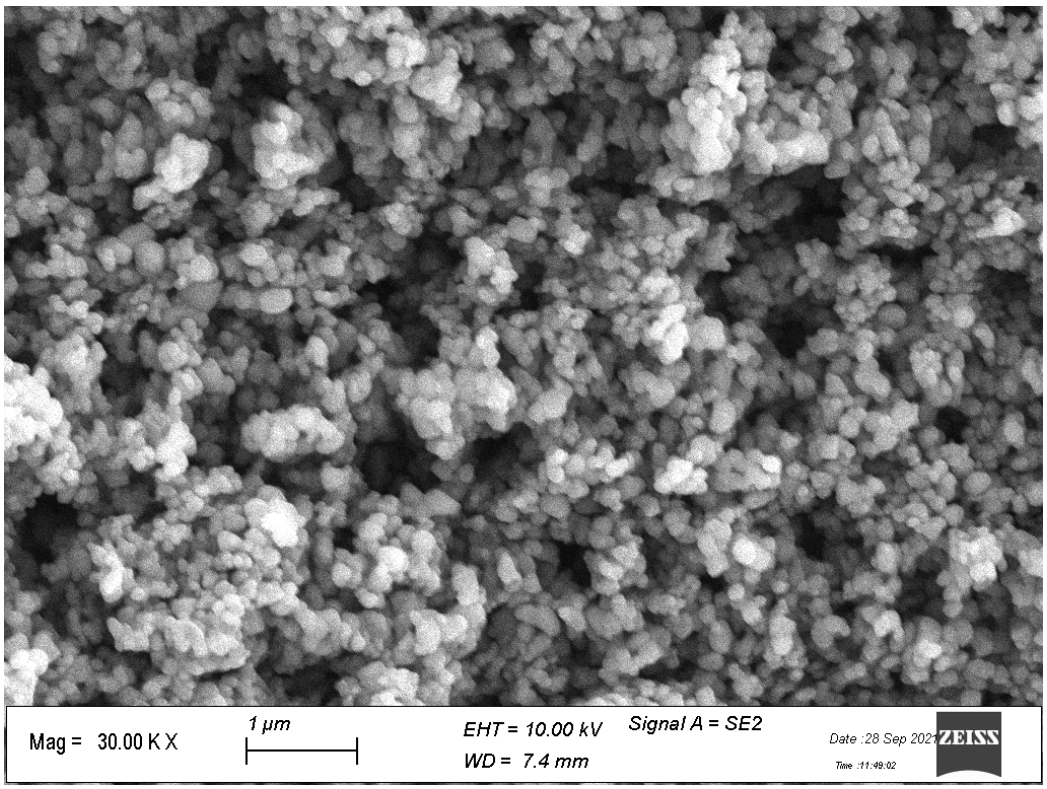

Figure 3. SEM image of a sample of TiO_2 and PVA deposition over vetronite at 30,000× magnification.

The electrical parameters involved in the discharge events were measured in the experiments. We used a Rogowski coil sensor to detect the current flowing in the system [24,25], and an HV probe to measure the associated applied high voltage.

The GC output reports a signal composed of peaks of intensity proportional to the concentration of specific species. The area of each peak is strongly dependent on the setting parameters during the sampling conditions. For a precise evaluation of concentration, we carried out a GC calibration with respect to pentane, considering the relative flow of pentane relative to the total air–pentane input flow. After calibration, we estimated the error in the pentane concentration to be around 10%. The errors were estimated as the standard deviation obtained from several measurements of the same starting concentration.

3. Experimental Results

To analyze the pentane depletion, we determined the resulting pentane concentrations based on the treatment time for various plasma conditions. The experimental campaign consisted of three steps: First, we opened the in-let and out-let valves in order to allow the pentane to flow through the reactor for two minutes. Second, the in-let and out-let valves were closed, after which the GC sampled the atmosphere in the reactor without plasma in order to measure the initial pentane concentration. Finally, in the third step, the plasma was turned on and kept working for a total time t, followed by a GC sampling of the treated gas. The treatment times t were taken in the range of 1–5 min. We repeated the process for each time t separately.

3.1. Gas Chromatograms

Several chromatogram measurements were repeated at different treatment times, plasma conditions, and pentane concentrations to improve the statistics of the results. The initial pentane concentrations chosen were $c = 300$, 600, 1200 ppm. The experiments were performed at two plasma power levels, i.e., 16.9 W and 44.2 W. We assigned c to be the nominal concentration that we add to the chamber, while ρ_5 represents the concentrations estimated by the GC sampling.

In Figure 4, we show a few examples of chromatograms. The initial pentane concentration was 1200 ppm, and the plasma was lit up at 44.2 W. We considered the two experimental conditions: depletion without a catalyst (Figure 4a) and depletion with a catalyst (Figure 4b).

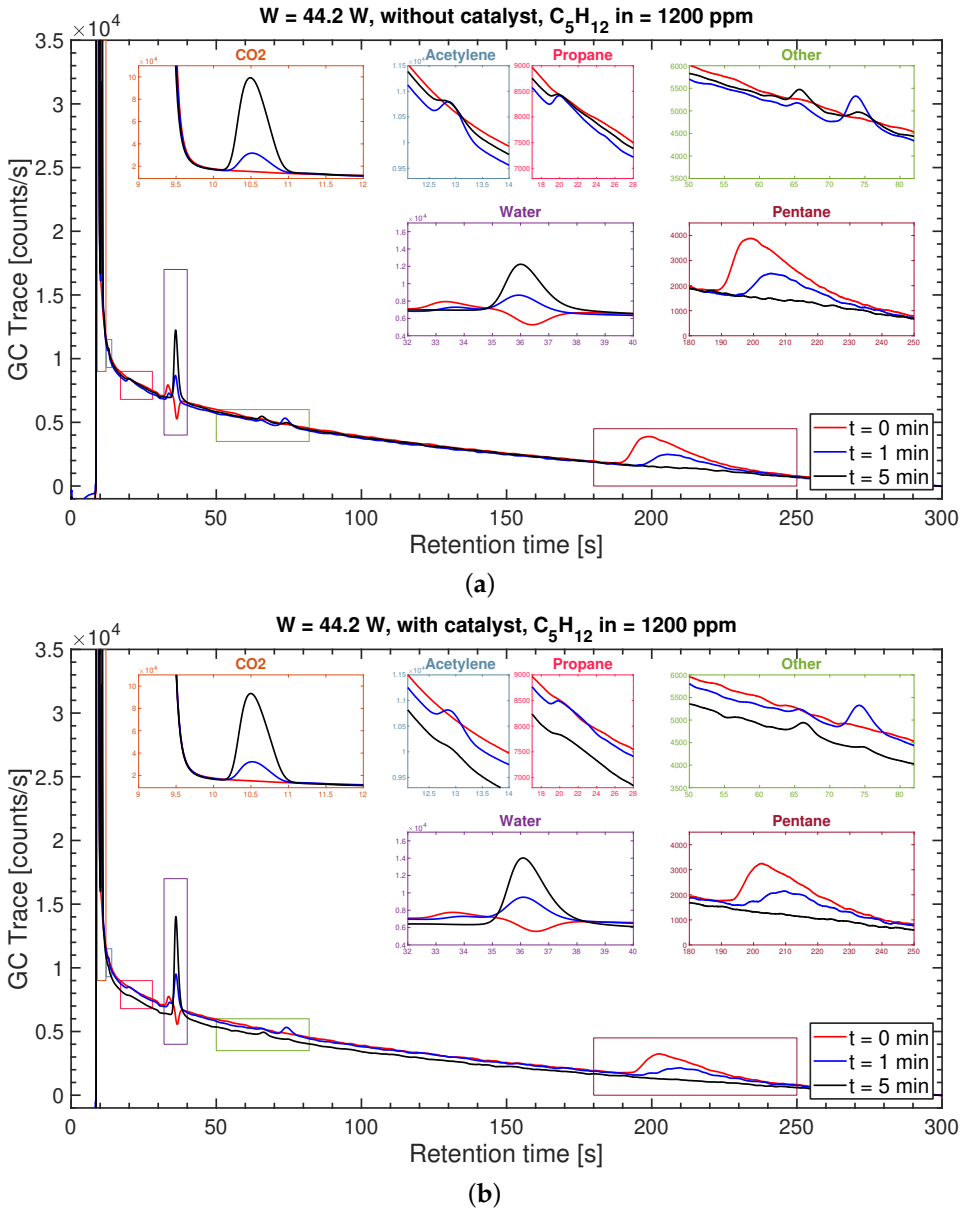

Figure 4. Gas chromatograms vs. retention time [s]. The shown traces correspond to pentane and intermediate products, for treatment times t = 0, 1, 5 min; the plasma lit up at 44.2 W, and initial pentane concentration was at 1200 ppm. (**a**) Without catalyst. (**b**) With catalyst. The duration of a gas chromatogram is 300 s. The insets show the traces for the intermediate reaction products (CO_2, acetylene, propane, water, and other unidentified species) and pentane.

The chromatograms shown in Figure 4a suggest that before the plasma treatment, except for the water peak, only the pentane peak was essentially present. After the plasma was switched on, the pentane concentration decreased, while intermediate reaction products such as carbon dioxide (CO_2), acetylene (C_2H_2), propane (C_3H_8), and water (H_2O) increased. The vertical positions of the lines are relative ones as they depend on the GC measurement. Only the peaks emerging from the red, blue, and black lines are relevant. It was not possible to identify other species, and their traces are reported in the upper right boxes of Figure 4.

In Figure 4b, we report the results in the presence of the catalyst. In both experimental conditions, pentane was completely abated after less than 5 min. It is interesting to note that the concentrations of some residual intermediates increased after 1 min of plasma treatment, while after 5 min, they were converted into CO_2 and water. We will discuss these features in Section 3.3.

3.2. Pentane Decomposition

In what follows, we analyze pentane depletion according to treatment time t, for the different experimental conditions, i.e., plasma power, initial pentane concentration, and catalyst activity. We found that relative to t, pentane concentration strongly depends on the plasma power used and on the catalyst activity. In particular, without the catalyst and at 16.9 W plasma power, pentane was almost fully, but not completely, decomposed after 5 min. However, at 44.2 W plasma power, a full decomposition took about 2 min.

It should be emphasized, however, that the full decomposition of pentane does not mean that pentane is completely converted to CO_2. As we discuss in Section 3.3, the plasma also produces intermediate reaction products such as acetylene and propane. In the presence of the catalyst, pentane is fully decomposed at the lower plasma power (16.9 W) in $t = 5$ min. At the higher plasma power (44.2 W), the catalyst activity is able to shorten the depletion time such that the pentane is completely decomposed in about 1 min.

To understand the chemical dynamics, we plotted the experimentally measured pentane concentrations (having an error of about 10%), $\rho_5(t)$, in Figure 5 relative to treatment time t. The basic idea here is to represent the data in semi-log scale in order to see whether the data are consistent with an exponential decay [26], either a single one or a more complex decay. We therefore used the following basic function:

$$\rho_5(t) = \rho_5(0)\, e^{-t/\tau_5}, \tag{1}$$

where $\rho_5(0)$ is the initial pentane concentration before plasma treatment, τ_5 is a parameter representing the characteristic time scale for depletion, which is related to the decomposition mean lifetime, $t_{1/2}$, according to $t_{1/2} = \tau_5 \log(2)$. As a general feature, we found that τ_5 depends on the initial pentane concentration.

As one can see from Figure 5a, the experimental values for the lower power, $P = 16.9$ W, scatter significantly. In particular, a double-exponential decay scenario seems to emerge at the initial pentane concentrations 600 ppm and 300 ppm. At the higher power of $P = 44.2$ W, considered in Figure 5b, the reduced time scale for depletion seems to be consistent with a single exponential decay for $\rho_5(t)$.

At plasma power $P = 16.9$ W, the reaction rates increase with decreasing initial pentane concentration (Figure 5a). At the highest pentane concentration (1200 ppm), we see a single decaying exponential, yielding a decomposition time of $\tau_5 = 5.3$ min. At lower pentane concentrations, the decay becomes faster, and a second regime seems to take place after $t = 2$ min. At these low concentrations and long times t, we expect the plasma to produce radical species more effectively. By increasing the residence time of the contaminated air in the plasma region (i.e., by prolonging the treatment time t), the availability of plasma-generated radical species for the air contaminant (pentane, in our case) increases. The availability of radical species becomes even higher when dealing with reduced concentrations of the air contaminant. Additional decomposition effects due to the catalyst are not apparent for pentane, such that pentane depletion seems to be dominated by the plasma to

a large extent. Given the uncertainties implied by the measurements, the present suggestion for a double-exponential decay remains to be understood. Additional measurements, which are beyond the scope of our work, are therefore required in order to draw a more quantitative conclusion.

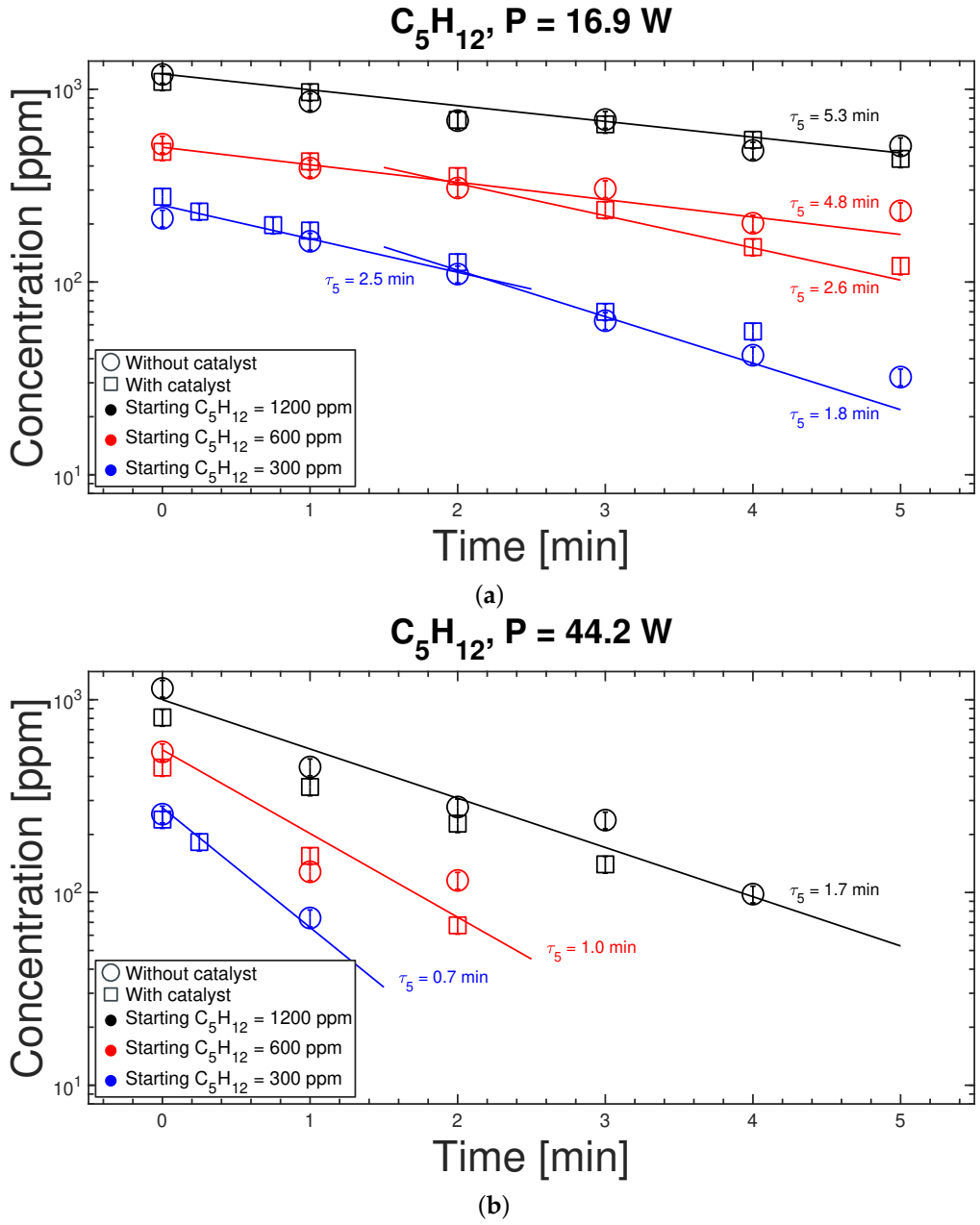

Figure 5. Depletion rate of pentane at different concentrations per plasma power: (**a**) $P = 16.9$ W, and (**b**) $P = 44.2$ W. The values for τ_5 (representing the slopes of the plotted straight lines) are summarized in Table 1 together with the estimated errors. The latter values were obtained by taking the highest and lowest slopes consistent with the data. The experimental uncertainties in the measured values, at about 10%, are roughly the size of the symbols shown.

At plasma power $P = 44.2$ W, much higher decomposition rates are found, and again, pentane depletion is plasma-dominated (Figure 5b). Now, we find single exponential decays for ρ_5. The fact that we only have three experimental points in Figure 5b for the low initial pentane concentrations is a result of the fast depletion rate found. One should consider intermediate treatment times to have more data points. However, the observed trend is sufficient to conclude that depletion is happening at a much higher rate. The straight

line shown, with a slope given by $\tau_5 = 0.7$ min, is consistent with the available data. Notice that we only have one parameter in the model, i.e., τ_5, and three times more data to fit it. Some deviations from the fit could be due to the presence of complex processes related to the generation of intermediate reaction products, as discussed below.

Quantitatively, pentane decomposition, denoted by D_5, is evaluated as follows:

$$D_5(\%) = 100\ \frac{[C_5H_{12}]_0 - [C_5H_{12}]_i}{[C_5H_{12}]_0}, \quad (2)$$

where $[C_5H_12]_0$ is the pentane concentration before treatment, and $[C_5H_12]_i$ is the pentane concentration after treatment time t. In Table 1, the pentane decomposition D_5 and the time scale for decomposition τ_5 are reported for $t = 5$ min in the absence and presence of the catalyst. As one can see for 44.2 W plasma power, pentane decomposition occurs in less than 2 min, and the depletion time scale τ_5 decreases with decreasing pentane concentrations, from 1.7 min (1200 ppm) to 0.7 min (300 ppm). Catalysis does not seem to compete with plasma at a high power level, and $D_5 > 95\%$. At the lower plasma power and for high pentane concentrations, neither the plasma nor the catalyst is able to completely abate pentane. At the lowest concentration, D_5 becomes larger than 95% in the presence of the catalyst. Indeed, the catalyst helps the depletion at low initial concentrations, while it does not greatly affect the depletion at higher concentrations. This can be explained by assuming that at high concentrations, the catalytic sites are saturated; therefore, the plasma controls the chemical kinetics.

Table 1. Pentane decomposition for the plasma treatment time $t = 5$ min, with and without a catalyst, for the two plasma powers and the three initial pentane concentrations considered in Figure 5. The associated pentane decomposition times, τ_5, are reported. The estimated errors for τ_5 are obtained by taking the highest and lowest slopes of the straight lines, consistent with the data shown in Figure 5.

Power (W)	Starting C_5H_{12} (ppm)	Catalyst	D_5 (%)	τ_5 (min)
16.9	300	No	87	2.5 ± 0.3 for $t < 2$ min, 1.8 ± 0.1 for $t > 2$ min
		Yes	>95	2.5 ± 0.3 for $t < 2$ min, 1.8 ± 0.1 for $t > 2$ min
	600	No	55	4.8 ± 0.5
		Yes	75	4.8 ± 0.5 for $t < 2$ min, 2.6 ± 0.2 for $t > 2$ min
	1200	No	58	5.3 ± 0.8
		Yes	60	5.3 ± 0.8
44.2	300	No	>95	0.7 ± 0.1
		Yes	>95	0.7 ± 0.1
	600	No	>95	1.0 ± 0.1
		Yes	>95	1.0 ± 0.1
	1200	No	>95	1.7 ± 0.2
		Yes	60	1.7 ± 0.2

We also estimated the pentane decomposition efficiency after 1 min of plasma treatment, displayed in Figure 6. The efficiency is estimated as the ratio between the amount in grams of the decomposed pentane to the applied energy in kWh. The efficiency increases with the pentane concentration, and the catalyst does not seem to play any relevant role in pentane decomposition, even at low concentrations. The increase in efficiency with pentane concentration demonstrates that for these plasma parameters, plasma processing occurs in the gas phase. These results are comparable to the efficiencies found in the NTP devices [10,27].

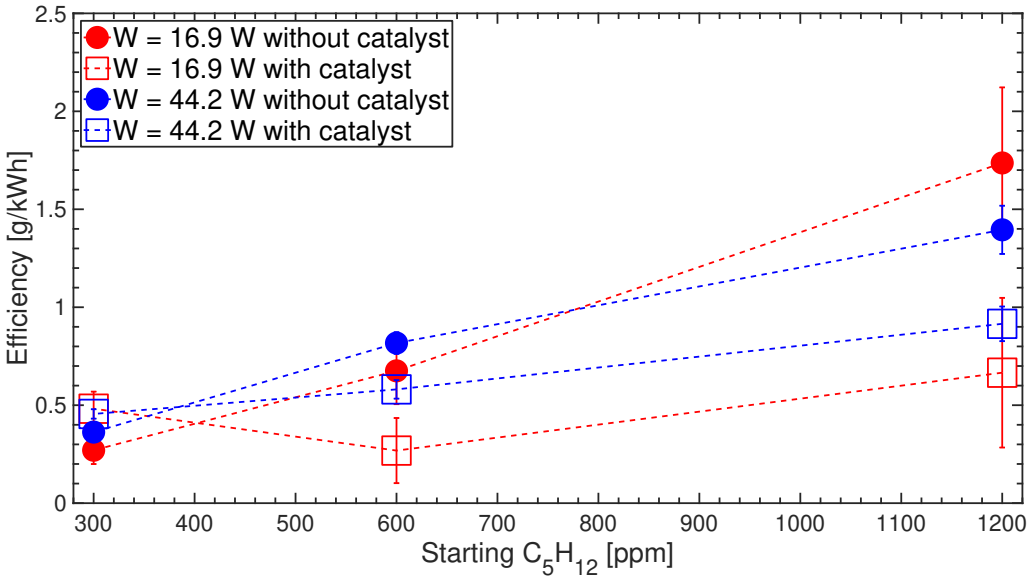

Figure 6. Pentane decomposition efficiency (g/kWh) after 1 min of plasma treatment according to the initial pentane concentration. The lines serve as visual guides. The error bars were obtained by calculating the error propagation in the estimation of the efficiency.

We also measured the ozone using the MQ131 ozone sensor coupled with Arduino Mega2560. We found that (in pure air, to avoid VOC sensor cross-sensitivity) for 16.9 W plasma power, the ozone was between 10 ppm and 20 ppm, while for 44.2 W, the ozone grew up to 400 ppm. The maximum efficiency of about 1.8 was obtained at the lower plasma power. At the higher plasma power, the fact that the efficiency was found to be smaller was probably due to the distribution of energy in the gas volume not being optimum at such higher power [28].

3.3. Intermediate Reaction Species

As shown in Figure 4, the plasma (acting for $t > 0$) shrinks the area of the pentane chromatogram peak, while other peaks appear. The water trace also changes as it depends on both the depletion processing, generated as by-products of VOC abatement species, and on the humidity transported by the chromatograph carrier gas (Helium). We could identify the acetylene and the propane peaks with the use of a calibration cylinder.

We were not able to identify the peaks classified as "Other" in Figure 4, which are suspected to be C_4 species, nor were we able to perform a CO_2 calibration. Thus, we will just concentrate on acetylene and propane here.

In order to fit the measured concentrations of the acetylene and propane species, denoted generically by x, we assume that the latter is regulated by a simple phenomenological differential equation consisting of a source term, proportional to $\rho_5(t)$, minus a loss term describing its extinction. The time evolution of the concentration $\rho_x(t)$ of species x is then given by the following equation:

$$\frac{d\rho_x(t)}{dt} = \frac{1}{\tau_{x5}}\rho_5(t) - \frac{1}{\tau_x}\rho_x(t), \tag{3}$$

where $\rho_5(t) = \rho_5(0)\exp(-t/\tau_5)$ (cf. Equation (1)), and x stands for acetylene or propane. Here, τ_{x5} represents the time scale for the generation of species x as a result of pentane decomposition, and τ_x is the time scale for the decomposition of the species x itself during the treatment. Thus, τ_{x5} and τ_x are the two parameters in the model.

The differential equation (Equation (3)) admits an exact solution, given by the equation below:

$$\frac{\rho_x(t)}{\rho_5(0)} = \frac{\tau_x\tau_5}{\tau_5 - \tau_x}\frac{1}{\tau_{x5}}\left(e^{-t/\tau_5} - e^{-t/\tau_x}\right). \tag{4}$$

In the case of an initial pentane concentration of $\rho_5(0) = 1200$ ppm, for the two plasma powers, with and without a catalyst, we obtain the $\tau_{x5,x}$ parameters by fitting the experimental data, as reported in Figure 7.

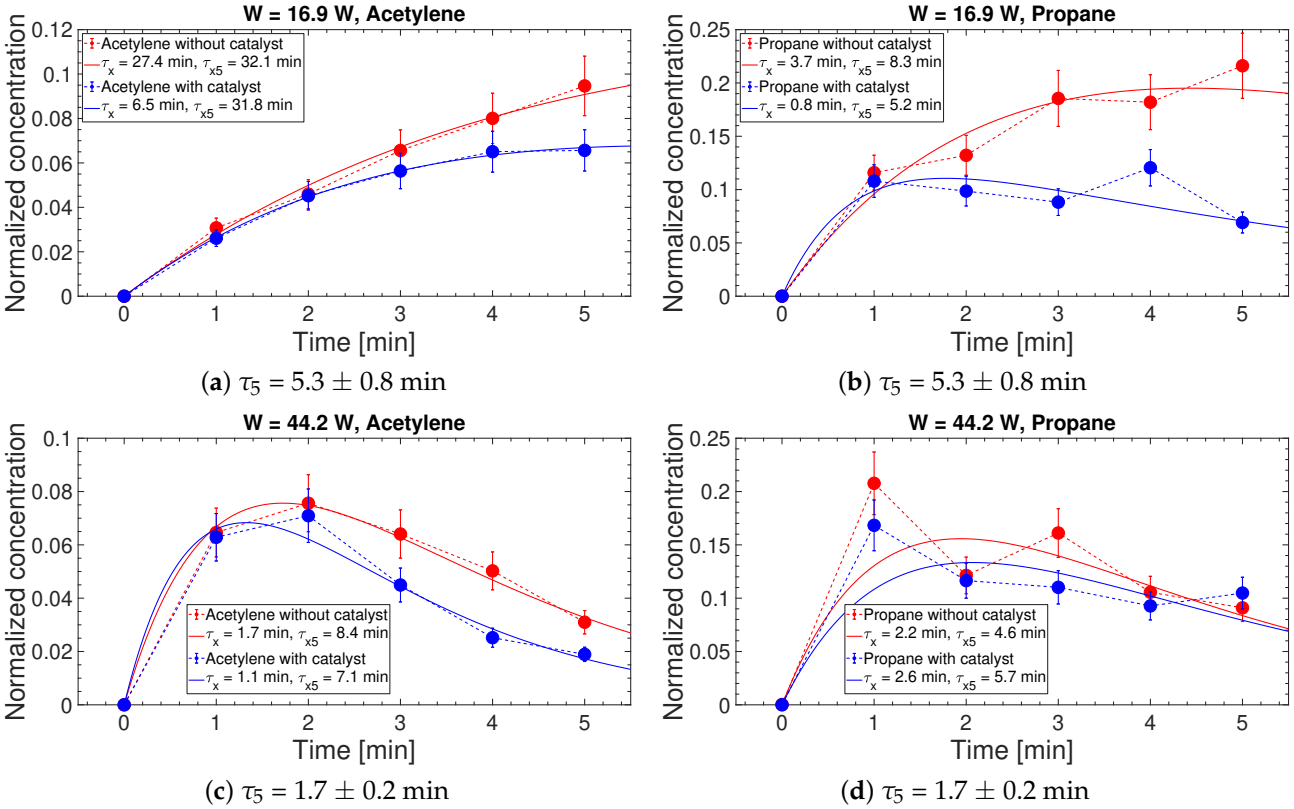

(**a**) $\tau_5 = 5.3 \pm 0.8$ min (**b**) $\tau_5 = 5.3 \pm 0.8$ min

(**c**) $\tau_5 = 1.7 \pm 0.2$ min (**d**) $\tau_5 = 1.7 \pm 0.2$ min

Figure 7. Normalized concentrations of intermediate products, acetylene, and propane, according to treatment time T (min), at 1200 ppm initial pentane concentration. (**a**,**c**) Acetylene at $P = 16.9$ W and $P = 44.2$ W, respectively. (**b**,**d**) Propane at $P = 16.9$ W and $P = 44.2$ W, respectively. The experimental uncertainties for the product concentrations were obtained by propagating the error due to the initial concentration of pentane yielding values equal to $\sqrt{2}$ 10%. The continuous lines are the results of the least-square fits obtained with Equation (4), while the dashed lines are just visual guides. The errors for τ_5 are from Table 1 (see also Figure 5). The errors associated with τ_x and τ_{x5} are those from the least-square fits and are reported in Table 2.

Table 2. Acetylene and propane characteristic times for different plasma treatments. The initial pentane concentration for this table corresponds to 1200 ppm. The errors for τ_x and τ_{x5} were obtained as discussed in Figure 7.

Specie	Power (W)	Catalyst	τ_5 (min)	τ_{x5} (min)	τ_x (min)
Acetylene	16.9	No	5.3 ± 0.8	32.1 ± 3.0	27.4 ± 8.0
		Yes	5.3 ± 0.8	31.8 ± 2.0	6.5 ± 1.0
	44.2	No	1.7 ± 0.2	8.4 ± 0.7	1.7 ± 0.2
		Yes	1.7 ± 0.2	7.1 ± 1.0	1.1 ± 0.1
Propane	16.9	No	5.3 ± 0.8	8.3 ± 2.0	3.7 ± 1.0
		Yes	5.3 ± 0.8	5.2 ± 2.0	0.8 ± 0.3
	44.2	No	1.7 ± 0.2	4.6 ± 1.0	2.2 ± 0.8
		Yes	1.7 ± 0.2	5.7 ± 2.0	2.6 ± 1.0

4. Discussion

A closer analysis of the results in terms of the time scales shown in Table 2 suggests that the catalyst is not directly involved in the decomposition of pentane. In fact, the time scales τ_5 are independent of the presence of the catalyst. At plasma power $P = 16.9$ W, $\tau_5 = (5.3 \pm 0.8)$ min, and at $P = 44.2$ W, $\tau_5 = (1.7 \pm 0.2)$ min, suggesting that the pentane decomposition is primarily due to the action of the plasma.

In contrast, the role of catalysts is very important for the depletion of the intermediate reaction products, as displayed by the associated time scales and denoted by τ_x, particularly at lower plasma power. For the latter, the catalytic depletion of intermediates is very efficient, as much as four times faster than that of plasma. Catalysis processing without plasma refers to an experiment where plasma is not switched on, and so only the catalyst (present on the surface of plasma module) is operating.

The reactions that the catalyst speeds up are the oxidation of acetylene and propane, which are previously formed by the partial decomposition of pentane, mainly by means of plasma action. At higher powers, the catalyst acts weakly on the depletion of acetylene, but not on propane. The time scale for the production of acetylene is weakly dependent on the catalyst, and at low power, it seems to diminish propane production.

These studies support the experimental evidence that catalysis concurs with the depletion of the intermediate reaction products in the plasma reactor, as also reported in the literature [29,30]. In the previous experiments reporting propane abatement, catalysis processing was used without a plasma, which showed very low efficiency. Therefore, the higher efficiency reported here is due to the synergetic effect of the plasma and the catalyst.

In fact, our previous study [31] demonstrated a much lower abatement efficiency for propane, performed by catalysis processing and using only UV-A light energy. In the case of TiO_2, we used light with a UV-A range of 340–400 nm and a peak at 370 nm to obtain an efficiency of less than 10% of the abatement after 22 min of application [31,32]. As previously reported in our studies, the UV-A power emitted by our SDBD was very low, from 20 to 600 times less bright in comparison with the typical UV-A lamps used for catalytic processing [33].

Other previous works suggested that introducing a catalyst into a plasma reactor could generate more highly energetic and reactive species, which favor plasma-induced reactions towards the deep oxidation of VOCs. In our case, the study of the kinematical evolution of depletion demonstrates that catalysts do not affect the pentane decomposition. We may conclude that the catalyst does not generate reactive species favoring the decomposition of the pentane, but it is the ability of the plasma state to primarily decompose pentane, thus generating the active intermediate species that could be removed by the catalyst. Catalytic processes are mainly responsible for removing the produced species, such as propane and acetylene, thus shifting the chemical kinetics towards full VOC depletion.

Hence, the combination of plasma with catalysis has a great potential to lower the activation temperature of the catalysts, enhance the removal of pollutants, and minimize the formation of undesired intermediate reaction products, all of which may contribute in different ways to the enhancement of the energy efficiency of the plasma process [27].

The results obtained in the present paper show that TiO_2 does not directly affect the removal/conversion of pentane, with the catalyst only having clear effects on the removal of excited species and by-products. The choice of the catalyst deserves further investigation in order to understand if different choices may influence the depletion of pentane. As an example, a recent study investigated the abatement of another alkane (n-undecane) and the related CO_x selectivity, achievable through the application of a packed-bed DBD reactor and using γ-Al_2O_3 spheres as packing material [34]. The removal efficiency of n-undecane and the CO_x selectivity increased from 40% to 80–92% and from 37% to 40–80%, respectively, when loading γ-Al_2O_3 with CeO_2 at different weight fractions.

In light of the numerous studies on cold atmospheric plasmas and their potentials for VOC abatement/conversion, such devices could be successfully employed in a broad spectrum of applications concerning VOC removal. The applications might be different

depending on the mode NTP devices used. Under static conditions, as in the present study, NTP devices show great potential in the decontamination of polluted environmental matrices such as contaminated air in confined volumes or contaminated soil [35].

NTP devices could also be applied to the treatment of contaminated air streams, thus under dynamic conditions. In this case, optimizing energy efficiency is a challenge that plasma technologies should face in the future, especially in applications regarding the treatment of high airflow rates. The use of catalysts, the combination with other removal technologies, or the study of peculiar configurations [36] may help to reduce the energy consumption in order to achieve the same targets.

The use of SDBD instead of volume DBDs also seems to be promising for energy optimization purposes. In a review paper, Vandenbroucke et al. [2] compared the results obtained by Oda et al. [37,38], who measured the abatement performance of trichloroethylene (TCE) by: (1) an SDBD reactor with a V_2O_5/TiO_2 catalyst, and (2) a volume DBD with a TiO_2 catalyst. At the same airflow rate (400 mL/min) and TCE concentration (1000 ppm), the first configuration allowed for the acquisition of the same removal efficiency for the second configuration (>95%) by using only 25–48% of the energy consumed by the latter. Other authors [39] carried out a comparison between an SDBD and a volume DBD reactor in terms of ozone generation. The authors found out that under the same operating conditions and specific energy density, the ozone generation obtained with the SDBD exceeds the amount of ozone generated by the volume DBD by a factor of 2.5–3.5. Similar results were obtained in a more recent study comparing the application of an SDBD and a volume DBD reactor to ethanol in air [40]. Under the same operating conditions and specific energy density, the authors obtained ethanol removal efficiencies of 80% and 60% when using the SDBD and the volume DBD reactor, respectively.

5. Conclusions

In this work, an SDBD reactor was employed for the decomposition of pentane, at different plasma discharge power levels (16.9 W and 44.2 W), gas concentrations in air, and plasma treatment time. It was found that pentane could be totally depleted in a few (about 5) minutes at 44.2 W, where the efficiency reaches the value of 1.3 g/kWh for the initial pentane concentration of 1200 ppm. The maximum efficiency of 1.8 g/kWh was found at 16.9 W, also for the initial pentane concentration of 1200 ppm. The efficiency increased with the pentane concentration, suggesting that plasma effects are volume-dependent because the reactions occurred in the gas phase. The fact that efficiency decreased with power suggests that plasma energy was either not well-distributed in the reactor or that the plasma produced a larger amount of by-products such as ozone, thus limiting other chemical reactions [28].

The analysis of the temporal evolution of pentane and the associated concentrations of the intermediate reaction products allowed us to quantitatively describe the kinetics of VOC depletion in the plasma hybrid system. In an SDBD–catalyst reactor, the plasma primarily acts to decompose pentane, while the catalyst mostly concerns the intermediate reaction products. During the first minutes of treatment in a single experiment, gas processing is dominated by plasma decomposition of pentane, followed by the generation of the intermediate products, which are progressively depleted by the catalytic processes acting on longer time scales.

Worthy of note is the fact that plasma dynamics depends on both the pentane concentration and applied power. It is faster at higher power and lower concentrations, where pentane is abated in less than 1 min. The typical time scale varies between 0.7 and 1.7 min for 300 ppm and 1200 ppm initial pentane concentrations, respectively. At extremely low powers, e.g., at 11 W, the pentane is not totally dissociated, and the time scale for abatement is longer, well above two minutes and roughly in the range of 2.5–5.3 min; this may be addressed by varying the concentrations between 300 ppm and 1200 ppm.

Different metal catalysts have been investigated in single-stage plasma-catalytic gas cleaning processes for the oxidation of VOCs. Transition metal oxide catalysts in combi-

nation with plasma have attracted growing interest for pollution abatement because of their comparable performance and low cost. In our previous work, we found that the TiO_2 and/or WO_3 catalysts alone are not able to efficiently remove propane [31], while here, we managed to increase the pentane depletion by using plasma together with a catalyst, thus yielding an efficient abatement of the intermediate reaction products.

Author Contributions: Conceptualization, C.R., C.P. and M.D.; methodology, C.R., C.P. and M.D.; software, C.P. and H.E.R.; validation, C.P.; formal analysis, C.P. and H.E.R.; investigation, C.P.; resources, C.R.; data curation, C.P.; writing—original draft preparation, C.R., C.P., H.E.R. and M.D.; writing—review and editing, C.R., C.P., H.E.R., M.D. and M.S.; visualization, C.P.; supervision, C.R.; project administration, C.R.; funding acquisition, C.R. All authors have read and agreed to the published version of the manuscript.

Funding: This research received no external funding.

Institutional Review Board Statement: Not applicable.

Informed Consent Statement: Not applicable.

Data Availability Statement: The data that support the findings of this study are available from the corresponding author upon reasonable request.

Acknowledgments: The authors gratefully acknowledge technical support from Alessandro Mietner and Alessandro Bau' in device development and experiment execution.

Conflicts of Interest: The authors declare no conflict of interest.

References

1. EEA. *Air Pollution*; European Environment Agency: Copenhagen, Denmark, 2017.
2. Vandenbroucke, A.; Morent, R.; De Geyter, N.; Leys, C. Non-thermal plasmas for non-catalytic and catalytic VOC abatement. *J. Hazard. Mater.* **2011**, *195*, 30–54. [CrossRef] [PubMed]
3. Aguayo-Villarreal, I.; Montes-Morán, M.; Hernández-Montoya, V.; Bonilla-Petriciolet, A.; Concheso, A.; Rojas-Mayorga, C.; González, J. Importance of iron oxides on the carbons surface vs the specific surface for VOC's adsorption. *Ecol. Eng.* **2017**, *106*, 400–408. [CrossRef]
4. Wang, W.; Ma, X.; Grimes, S.; Cai, H.; Zhang, M. Study on the absorbability, regeneration characteristics and thermal stability of ionic liquids for VOCs removal. *Chem. Eng. J.* **2017**, *328*, 353–359. [CrossRef]
5. Donley, E.; Lewandowski, D. Optimized Design and Operating Parameters for Minimizing Emissions During VOC Thermal Oxidation. *Met. Finish. Guideb.-Dir.* **1998**, *96*, 52–58. [CrossRef]
6. Chen, X.; Carabineiro, S.; Bastos, S.; Tavares, P.; Órfão, J.; Pereira, M.; Figueiredo, J. Catalytic oxidation of ethyl acetate on cerium-containing mixed oxides. *Appl. Catal. A Gen.* **2014**, *472*, 101–112. [CrossRef]
7. Vergara-Fernández, A.; Revah, S.; Moreno-Casas, P.; Scott, F. Biofiltration of volatile organic compounds using fungi and its conceptual and mathematical modeling. *Biotechnol. Adv.* **2018**, *36*, 1079–1093. [CrossRef]
8. Belaissaoui, B.; Le Moullec, Y.; Favre, E. Energy efficiency of a hybrid membrane/condensation process for VOC (Volatile Organic Compounds) recovery from air: A generic approach. *Energy* **2016**, *95*, 291–302. [CrossRef]
9. Schiavon, M.; Torretta, V.; Casazza, A.; Ragazzi, M. Non-thermal plasma as an innovative option for the abatement of volatile organic compounds: A review. *Water Air Soil Pollut.* **2017**, *228*, 1–20. [CrossRef]
10. Li, S.; Dang, X.; Yu, X.; Abbas, G.; Zhang, Q.; Cao, L. The application of dielectric barrier discharge non-thermal plasma in VOCs abatement: A review. *Chem. Eng. J.* **2020**, *388*, 124275. [CrossRef]
11. Dobslaw, C.; Glocker, B. Plasma Technology and Its Relevance in Waste Air and Waste Gas Treatment. *Sustainability* **2020**, *12*, 8981. [CrossRef]
12. Shin, D.; Hong, Y.; Lee, S.; Kim, Y.; Cho, C.; Ma, S.; Chun, S.; Lee, B.; Uhm, H. A pure steam microwave plasma torch: Gasification of powdered coal in the plasma. *Surf. Coat. Technol.* **2013**, *228*, S520–S523. [CrossRef]
13. Choi, S.; Hong, S.; Lee, H.; Watanabe, T. A comparative study of air and nitrogen thermal plasmas for PFCs decomposition. *Chem. Eng. J.* **2012**, *185*, 193–200. [CrossRef]
14. Suris, A. Investigation of high-temperature steam-air reagents for plasma waste treatment processes. *Theor. Found. Chem. Eng.* **2017**, *51*, 348–351. [CrossRef]
15. George, A.; Shen, B.; Craven, M.; Wang, Y.; Kang, D.; Wu, C.; Tu, X. A Review of Non-Thermal Plasma Technology: A novel solution for CO_2 conversion and utilization. *Renew. Sustain. Energy Rev.* **2021**, *135*, 109702. [CrossRef]
16. Pietanza, L.; Colonna, G.; Capitelli, M. Kinetics versus thermodynamics on CO_2 dissociation in high temperature microwave discharges. *Plasma Sources Sci. Technol.* **2020**, *29*, 035022. [CrossRef]

17. Dobslaw, D.; Ortlinghaus, O.; Dobslaw, C. A combined process of non-thermal plasma and a low-cost mineral adsorber for VOC removal and odor abatement in emissions of organic waste treatment plants. *J. Environ. Chem. Eng.* **2018**, *6*, 2281–2289. [CrossRef]
18. Barni, R.; Benocci, R.; Spinicchia, N.; Roman, H.; Riccardi, C. An experimental study of plasma cracking of methane using DBDs aimed at hydrogen production. *Plasma Chem. Plasma Process.* **2019**, *39*, 241–258. [CrossRef]
19. Long, H.; Shang, S.; Tao, X.; Yin, Y.; Dai, X. CO_2 reforming of CH_4 by combination of cold plasma jet and Ni/γ-Al_2O_3 catalyst. *Int. J. Hydrogen Energy* **2008**, *33*, 5510–5515. [CrossRef]
20. Piferi, C.; Barni, R.; Roman, H.; Riccardi, C. Current Filaments in Asymmetric Surface Dielectric Barrier Discharge. *Appl. Sci.* **2021**, *11*, 2079. [CrossRef]
21. Abdelaziz, A.; Seto, T.; Abdel-Salam, M.; Otani, Y. Performance of a surface dielectric barrier discharge based reactor for destruction of naphthalene in an air stream. *J. Phys. D Appl. Phys.* **2012**, *45*, 115201. [CrossRef]
22. Assadi, A.; Bouzaza, A.; Wolbert, D. Comparative study between laboratory and large pilot scales for VOC's removal from gas streams in continuous flow surface discharge plasma. *Chem. Eng. Res. Des.* **2016**, *106*, 308–314. [CrossRef]
23. Siliprandi, R.; Roman, H.; Barni, R.; Riccardi, C. Characterization of the streamer regime in dielectric barrier discharges. *J. Appl. Phys.* **2008**, *104*, 063309. [CrossRef]
24. Biganzoli, I.; Barni, R.; Riccardi, C. Note: On the use of Rogowski coils as current probes for atmospheric pressure dielectric barrier discharges. *Rev. Sci. Instrum.* **2013**, *84*, 016101. [CrossRef] [PubMed]
25. Biganzoli, I.; Barni, R.; Gurioli, A.; Pertile, R.; Riccardi, C. Experimental investigation of Lissajous figure shapes in planar and surface dielectric barrier discharges. *J. Phys. Conf. Ser.* **2014**, *550*, 012039. [CrossRef]
26. Kim, H. Nonthermal plasma processing for air-pollution control: A historical review, current issues, and future prospects. *Plasma Process. Polym.* **2004**, *1*, 91–110. [CrossRef]
27. Chung, W.; Mei, D.; Tu, X.; Chang, M. Removal of VOCs from gas streams via plasma and catalysis. *Catal. Rev.* **2019**, *61*, 270–331. [CrossRef]
28. Nguyen, H.; Park, M.; Kim, S.; Kim, H.; Baik, L.; Jo, Y. Effective dielectric barrier discharge reactor operation for decomposition of volatile organic compounds. *J. Clean. Prod.* **2018**, *198*, 1232–1238. [CrossRef]
29. Shayegan, Z.; Lee, C.; Haghighat, F. TiO_2 photocatalyst for removal of volatile organic compounds in gas phase—A review. *Chem. Eng. J.* **2018**, *334*, 2408–2439. [CrossRef]
30. Feng, X.; Liu, H.; He, C.; Shen, Z.; Wang, T. Synergistic effects and mechanism of a non-thermal plasma catalysis system in volatile organic compound removal: A review. *Catal. Sci. Technol.* **2018**, *8*, 936–954. [CrossRef]
31. Piferi, C.; Riccardi, C. High concentration propane depletion with photocatalysis. *AIP Adv.* **2021**, *11*, 125008. [CrossRef]
32. Bin, Z.; Zhang, L.; Yan, Y.; Meng, L.; Yimin, Z. Enhancing toluene removal in a plasma photocatalytic system through a black TiO_2 photocatalyst. *Plasma Sci. Technol.* **2019**, *21*, 115503.
33. Piferi, C.; Brescia, A.; Riccardi, C. Intensity comparison between UV lamps and plasma emission for air purification studies. *AIP Adv.* **2021**, *11*, 085209. [CrossRef]
34. Xia, T.; Yao, S.; Wu, Z.; Li, G.; Li, J. High ratio of $Ce^{3+}/(Ce^{3+}+Ce^{4+})$ enhanced the plasma catalytic degradation of n-undecane on CeO_2/γ-Al_2O_3. *J. Hazard. Mater.* **2022**, *424*, 127700. [CrossRef] [PubMed]
35. Aggelopoulos, C.; Svarnas, P.; Klapa, M.; Tsakiroglou, C. Dielectric barrier discharge plasma used as a means for the remediation of soils contaminated by non-aqueous phase liquids. *Chem. Eng. J.* **2015**, *270*, 428–436. [CrossRef]
36. Martini, L.; Coller, G.; Schiavon, M.; Cernuto, A.; Ragazzi, M.; Dilecce, G.; Tosi, P. Non-thermal plasma in waste composting facilities: From a laboratory-scale experiment to a scaled-up economic model. *J. Clean. Prod.* **2019**, *230*, 230–240. [CrossRef]
37. Oda, T.; Takahashi, T.; Kohzuma, S. Decomposition of Dilute Trichloroethylene by Using Nonthermal Plasma Processing. *IEEE Trans. Ind. Appl.* **2001**, *37*, 965–970. [CrossRef]
38. Oda, T.; Takahahshi, T.; Yamaji, K. Nonthermal plasma processing for dilute VOCs decomposition. *IEEE Trans. Ind. Appl.* **2002**, *38*, 873–878. [CrossRef]
39. Nassour, K.; Brahami, M.; Nemmich, S.; Hammadi, N.; Zouzou, N.; Tilmatine, A. Comparative experimental study between surface and volume DBD ozone generator. *Ozone Sci. Eng.* **2016**, *38*, 70–76. [CrossRef]
40. Nobrega, P.; Blin-Simiand, N.; Bournonville, B.; Jorand, F.; Lacour, B.; Pasquiers, S.; Rohani, V.; Cauneau, F.; Fulcheri, L. Comparison between performances of surface and volume nanosecond pulsed dielectric barrier discharges for the treatment of volatile organic compounds. In Proceedings of the 23rd International Symposium on Plasma Chemistry-ISPC 23, Montréal, QC, Canada, 30 July 2017.